Time-domain analysis of transient structural acoustics problems based on the finite element method and a novel absorbing boundary element

Loukas F. Kallivokas and Jacobo Bielak
Computational Mechanics Laboratory, Department of Civil Engineering, Carnegie Mellon University, Pittsburgh, Pennsylvania 15213

(Received 1 March 1993; revised 27 August 1993; accepted 30 August 1993)

This paper is concerned with the development of an efficient and accurate finite element procedure for the solution directly in the time domain of transient problems involving structures submerged in an infinite acoustic fluid. The central feature of the procedure is a novel impedance, or, absorbing boundary, element that is used to render the computational domain finite. This element is local in both time and space, and is completely defined by a pair of symmetric stiffness and damping matrices. It thus can be attached directly to the adjoining fluid elements within the computational domain using standard assembly procedures. Due to its local nature, it also preserves the overall structure of the global equations of motion, including symmetry and sparseness. Thus the new impedance element makes it possible to solve complex transient exterior structural acoustics problems via existing finite element software for interior problems by just incorporating this element into current finite element libraries. Standard step-by-step temporal integration techniques can then be used to solve the resulting equations of motion. Even though the focus is in the time domain, the same equations of motion can naturally be used to determine the solution under time-harmonic excitation directly in the frequency domain. In this paper the new methodology is presented in a two-dimensional setting, using as a model an infinite cylindrical thin elastic circular shell submerged in an acoustic fluid. The absorbing element, however, can be used equally well with any arbitrary (possibly nonlinear) two-dimensional structure. Explicit formulas for the element matrices are included, and numerical examples, involving both transient scattering and radiation model problems, are given for the homogeneous shell as well as for a shell with a concentrated mass to illustrate the validity and accuracy of the new procedure.

PACS numbers: 43.20.Px, 43.20.Tb, 43.30.Jx, 43.40.Rj

INTRODUCTION

To date the overwhelming majority of investigations dealing with problems in structural acoustics have focused on the steady-state response of the fluid–structure system to time-harmonic excitation; it is thus natural that solutions have been carried out primarily in the frequency domain. While frequency-domain analyses are often sufficient in practice, there are situations for which an analysis directly in the time domain may be desirable or even unavoidable. Clearly, a time-domain approach provides the only practical alternative if any part of the structure can behave inelastically. Also, given that measurements of experimental or actual performance of fluid–structure interaction systems are recorded directly in the time domain, it may be of interest in some cases, say for purposes of structural or noise control or optimum structural design, to either use or compare this information with that predicted directly by the mathematical models.

With these applications in mind, this paper is concerned with the ultimate development of efficient, yet accurate, numerical techniques for evaluating directly in the time domain the transient response of (possibly inelastic) structures of complex geometry submerged in an infinite (or semi-infinite) acoustic medium. The excitation can be exterior, e.g., in the form of prescribed incident pressure waves propagating through the fluid (scattering problem), or interior, due to forces generated within the structure itself (radiation problem). In contrast to the vast literature available for time-harmonic problems (see, e.g., Refs. 1–4 for a partial list of relevant studies) transient problems in exterior structural acoustics have received scanty attention. Whereas an exact boundary integral formulation for transient problems in terms of retarded potentials is possible, the direct application of this procedure to realistic problems is generally impractical due to the nonlocal nature of this formulation both in time and in space; that is, in this approach the response at every point on the fluid–structure interface depends on the complete history of the response at every other point. An alternative approach is to truncate the infinite domain and to specify a boundary condition on the artificial boundary that will satisfy approximately the radiation condition. The goal is to arrive at boundary conditions that are more local, at least in time.

A survey of various absorbing boundary treatments up

 0001-4966/93/94(6)/3480/13/$6.00

to 1990 is given by Givoli.[5] Here we mention the well-known sequences of boundary conditions obtained by Engquist and Majda[6] and Bayliss and Turkel[7] using rational approximations to pseudodifferential operators and asymptotic expansions of the radial distance, respectively. A finite element scheme for solving the acoustic radiation problem using Bayliss and Turkel's second-order approximation has been implemented by Pinsky *et al.*[8] and by Pinsky and Abboud[9,10] for two- and three-dimensional problems, respectively. Numerical results were presented in these papers for various uniform and nonuniform Dirichlet exterior problems and for the axisymmetric radiation problem involving an elastic infinite cylindrical shell subject to a uniform internal pressure; the Bayliss–Turkel second-order condition was also incorporated formally into the symmetric formulation of the complete structure–fluid interaction problem developed originally by Everstine[11] without any numerical examples; it should be added that the nonsymmetric character of the boundary treatment in Refs. 8–10 destroys the symmetry of the global equations. An example of an application based on an alternative boundary treatment, the doubly asymptotic approximation (DAA), is given in Ref. 12 for the case of an infinite cylindrical shell with appendages. This approach,[13–17] which combines an early time with a late time approximation, allows one to enforce the absorbing boundary condition directly on the interface of the structure with the fluid. The price one pays for this benefit, however, is having to deal with a spatially nonlocal boundary, since at each instant the DAA causes the response at each point of the boundary to be coupled with that at every other point.

Barry *et al.*[18] have developed a family of approximate local boundary conditions for the transient two-dimensional wave equation using ideas of geometrical optics. For a particular value of a parameter their second-order condition coincides with the corresponding second-order Bayliss–Turkel condition. By giving it a viscoelastic interpretation, Kallivokas *et al.*[19] were able to recast the second-order condition of Barry *et al.* into an equivalent form that can be represented completely, upon discretization, by a very simple boundary element, local in time and space. The practical significance of this novel impedance element, which can be completely characterized by a pair of stiffness and damping symmetric matrices, is that it makes it possible, apparently for the first time, to solve accurately and efficiently exterior initial-value problems in structural acoustics, and other multiphase phenomena, with existing finite element software for interior problems.

The main objective of the present paper is to demonstrate how this approach can be applied readily to the solution of the exterior two-dimensional structural acoustics problem. To preserve symmetry we formulate the problem variationally in terms of the displacement field and the velocity potential field introduced originally by Everstine,[11] for the structure and the fluid, respectively. We concentrate on the infinite cylindrical thin elastic shell, using this canonical geometry as a benchmark since the corresponding transient scattering problem is amenable to exact solution. Arbitrary elastic structures can be analyzed similarly merely by modifying the expression for the strain energy in the variational principle. We present numerical results for scattering and radiation problems for the homogeneous shell and for a limiting rigid scatterer, as well as for a shell with a concentrated line mass, using a finite-duration modified Ricker[20] pulse as the excitation. The Ricker pulse, used frequently in seismology, has the property that the amplitude of its Fourier transform has a single well-defined dominant frequency, and has nonzero values only over a prescribed frequency band. Thus, the pulse can be tuned to excite the structure–fluid system up to a desired maximum frequency.

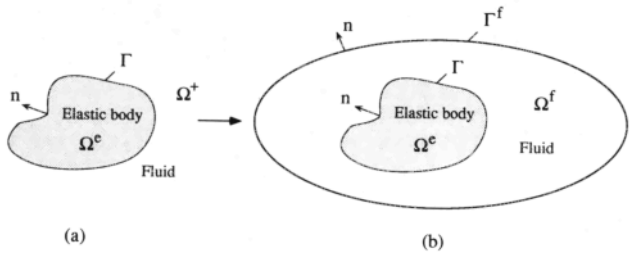

FIG. 1. (a) Model of fluid–structure interaction system. (b) Reduced model with finite fluid region and absorbing boundary.

I. PROBLEM DESCRIPTION AND ABSORBING BOUNDARIES

We discuss initially the general case of an arbitrary two-dimensional elastic structure submerged in an infinite acoustic medium and subsequently present a detailed derivation for the cylindrical shell. Suppose Ω^e represents the region occupied by the structure, Ω^+ the corresponding exterior region, and Γ their interface, as shown in Fig. 1(a). We assume that the homogeneous, compressible, and inviscid fluid remains close to an equilibrium state with constant density and velocity. Then the linearized equations of motion for the fluid are

$$\rho \dot{\mathbf{v}}^f = -\nabla P, \tag{1a}$$

$$\dot{\rho} + \rho \nabla \cdot \mathbf{v}^f = 0, \tag{1b}$$

$$\rho = (1/c^2) P, \tag{1c}$$

where $\mathbf{v}^f$ is the velocity vector, P is the total pressure, ρ is the density, and c is the speed of sound in the acoustic medium. We assume there is an incident transient fluid motion given by a pressure p^0, where p^0 satisfies the wave equation with speed of sound c; the simple modifications needed to consider the corresponding radiation problem will be discussed later. Following Everstine,[11] we introduce the velocity potential function ψ through the following relationships:

$$\mathbf{v}^f = \nabla \psi - \frac{1}{\rho} \nabla \int_0^t p^0 \, dt, \tag{2a}$$

$$P = -\rho \dot{\psi} + p^0. \tag{2b}$$

With this choice of ψ, $-\rho\dot{\psi}$ represents the scattered pressure and (1a) is satisfied automatically. Equations (1b)

and (1c) also will be satisfied for a system which is initially at rest provided ψ satisfies the wave equation:

$$c^2\nabla^2\psi=\ddot{\psi}. \tag{3}$$

Since the scattered wave $-\rho\dot{\psi}$ must be outgoing, then ψ must satisfy a radiation condition at infinity. Rather than considering the structural acoustic scattering problem over the infinite domain $\mathscr{R}^2$, we introduce an artificial, smooth, convex boundary Γ^f in Ω^+ and pose an equivalent problem over the finite region $\Omega^e\cup\bar{\Omega}^f$, as shown in Fig. 1(b). Then on Γ^f, ψ will satisfy an exact nonlocal condition for the normal derivative, $\psi_n=\nabla\psi\cdot\mathbf{n}$, where $\mathbf{n}$ is the unit outer normal to Γ^f, of the form:

$$\psi_n=\mathscr{F}[\psi^t(\cdot,\cdot)](x,t),\ \text{on}\ \Gamma^f. \tag{4}$$

The right side denotes a functional of the values of $\psi(\xi,\zeta)$ for ξ ranging over Γ^f and ζ from 0 to t. Hence, $\mathscr{F}$ is the exact operator expressing the spatial and temporal nonlocality on Γ^f. In other words, $\mathscr{F}$ merely expresses the fact that at a given instant t the motion at every point on the artificial boundary Γ^f is coupled with the time histories of all other points on Γ^f. Theoretically, one could obtain $\mathscr{F}$ by solving (3) in the exterior region Ω^+ for given values $\psi|_{\Gamma^f}$ on Γ^f and then computing the normal derivative on Γ^f. Even if this were possible the relationship (4) would not be too practical due to its nonlocal behavior.

The idea then is to approximate $\mathscr{F}$ so as to reduce the temporal nonlocality. Using geometrical optics to obtain an (exact) asymptotic expansion of the Laplace transform of $\mathscr{F}$ for large values of the transform parameter s, Barry *et al.*[18] obtained a sequence of approximations for $\mathscr{F}$. The first three approximations are:

$$\psi_n=-\frac{1}{c}\dot{\psi}, \tag{5a}$$

$$\psi_n=-\frac{1}{c}\dot{\psi}+\frac{1}{2}\kappa\psi, \tag{5b}$$

$$\dot{\psi}_n+\delta\psi_n=-\frac{1}{c}\ddot{\psi}+\left(\frac{1}{2}\kappa-\frac{\delta}{c}\right)\dot{\psi}+\frac{1}{2}c\psi_{\lambda\lambda}+(\tfrac{1}{8}\kappa^2c+\tfrac{1}{2}\kappa\delta)\psi, \tag{5c}$$

in which κ=curvature of Γ^f, the subscript λ denotes differentiation with respect to the arc length, and δ is an arbitrary parameter that for stability must be greater than a certain critical value δ_{cr}.

The first approximation is identical to the Mindlin and Bleich[21] plane wave approximation (PWA), while for a circle the second one coincides with the first-order expression from Bayliss and Turkel.[7] Physically, (5a) corresponds to a set of dashpots on the artificial boundary while (5b) represents a set of Voigt elements with springs and dashpots in parallel. It is noteworthy that for $\delta=-c\kappa$, (5c) reduces to an approximation derived by Kriegsmann *et al.*,[22] while for the special case of a circle (5c) also reduces to the second-order condition derived by Bayliss and Turkel[7] provided one chooses $\delta=4\delta_{cr}$ ($\delta_{cr}=c/4R$), where R is the radius of the circle. We remark that the Laplace transform of (4) agrees with that of (5c) through terms of order s^{-2}; hence the designation of second order for the latter approximation.

Equation (5c), or any of its particular cases, can be used directly for numerical applications, as was done in Ref. 8. This equation, however, has the disadvantage that it contains a linear combination of ψ_n and its time derivative $\dot{\psi}_n$ rather than being expressed in terms of ψ_n by itself, as required in a variational formulation. This has the consequence of destroying the symmetry of the original problem (and perhaps also decreasing the accuracy of the numerical procedure) since (5c) requires that $\dot{\psi}_n$ be approximated numerically.

By giving (5c) a physical interpretation borrowed from viscoelasticity in terms of springs and dashpots, Kallivokas *et al.*[19] were able to show that this equation can be rewritten as:

$$\psi_n=-\frac{1}{c}\dot{\psi}+\frac{\kappa}{2}\psi+\frac{\kappa^2c}{8\delta}\psi^{(1)}+\frac{c}{2\delta}\psi^{(2)}_{\lambda\lambda}, \tag{6a}$$

where $\psi^{(1)}$ and $\psi^{(2)}$ are two auxiliary variables, which are related to ψ by

$$\frac{\kappa^2c}{8\delta}(\psi-\psi^{(1)})=\frac{\kappa^2c}{8\delta^2}\dot{\psi}^{(1)}, \tag{6b}$$

$$\frac{c}{2\delta}(\psi_{\lambda\lambda}-\psi^{(2)}_{\lambda\lambda})=\frac{c}{2\delta^2}\dot{\psi}^{(2)}_{\lambda\lambda}. \tag{6c}$$

Now, (6a) has the desired form. Even though it contains two new variables and the introduction of these variables adds two new equations to the formulation, the set of equations (6) can be readily incorporated into a variational formulation.

Thus the structural acoustics problem, in its exact formulation, consists in solving the equations of elastodynamics for the displacement field within Ω^e and the wave equation (3) in Ω^f for the velocity potential field, under zero initial conditions, due to the incident pressure p^0. In addition the traction and the normal velocity must be continuous across the interface Γ and ψ must satisfy the radiation condition (4). Here, p^0 and its normal derivative enter into the formulation through the transition conditions across Γ. For the approximate problem we replace (4) by either (5a), (5b), or (6).

II. VARIATIONAL FORMULATION

In order to derive a finite element approximation for the structural acoustics problem described in the preceding section it is desirable to have a variational formulation of the problem. In this section we develop a direct variational formulation for the particular case of an infinitely long cylindrical shell, using Hamilton's principle as a point of departure. We consider this canonical shell for clarity and convenience, so that later on we may assess the accuracy of our numerical approximations through comparisons with exact solutions. To extend the procedure to an arbitrary

two-dimensional elastic structure one need only use the appropriate expressions for the strain energy of the given structure in the following formulation.

Consider an infinitely long cylindrical shell of thickness d and radius a referred to an (r,θ,z) polar coordinate system. The corresponding displacements of the shell at midsurface are w, v, and u. We assume that the incident wave p^0 acts normally to the cylindrical surface of the shell and is independent of the coordinate z; this gives rise to a plane-strain state in which the axial component of displacement u vanishes and the circumferential and radial components v and w, respectively, are independent of the axial coordinate z. We use the thin shell theory as presented by Junger and Feit.[23]

For this shell–fluid system, Hamilton's principle can be expressed as

$$\delta\int_{t_1}^{t_2}(T_s+T_f-V_s-V_f)dt$$
$$=-\int_{t_1}^{t_2}\left(-\int_\Gamma P\delta w\,ds+\int_\Gamma(\mathbf{u}^f\cdot\mathbf{n})\delta P\,ds\right.$$
$$\left.-\int_{\Gamma^f}(\mathbf{u}^f\cdot\mathbf{n})\delta P\,ds\right)dt, \tag{7}$$

where[23]

$$T_s=\frac{1}{2}\rho_s d\int_\Gamma(\dot v^2+\dot w^2)d\lambda, \tag{8a}$$

$$T_f=\frac{1}{2}\rho\int_{\Omega^f}\mathbf{v}^f\cdot\mathbf{v}^f d\Omega, \tag{8b}$$

$$V_s=\frac{1}{2}\frac{Ed}{1-\nu^2}\frac{1}{a^2}\int_\Gamma[(v_\phi+w)^2+\beta^2(w_{\phi\phi}-v_\phi)^2]d\lambda, \tag{8c}$$

$$V_f=\frac{1}{2\rho c^2}\int_{\Omega^f}P^2\,d\Omega. \tag{8d}$$

Here, ρ_s, E, and ν, are the mass density, Young's modulus, and Poisson's ratio of the shell, $\beta^2=d^2/12a^2$, subscript ϕ denotes partial derivative in the circumferential direction, t_1 and t_2 are two arbitrary instants, $\mathbf{u}^f$ is the displacement within the fluid ($\dot{\mathbf{u}}^f=\mathbf{v}^f$), and the differential of arc length $d\lambda$ is equal to $ad\phi$. Equation (7) is a statement of the condition that the sum of the variation of the Lagrangian must be equal to the negative of the virtual work done by external agents acting on each subsystem. Here, T_s and T_f are the kinetic energy in the shell and fluid, respectively, V_s is the strain energy in the shell, and V_f the potential energy in the fluid. The first integral on the right is the virtual work done on the shell by the fluid pressure, while the second and third terms represent the corresponding work on the inner and outer boundaries of the fluid.

If one substitutes (2), (8), and the exact boundary condition (4) on Γ^f into (7), it can be shown that after: (a) performing the indicated variation on the left side; (b) integrating by parts with respect to time, as necessary under the temporary assumption that the virtual quantities δv, δw, $\delta\psi$ vanish at the two limits t_1 and t_2; (c) recalling that p^0 satisfies the wave equation in the fluid; and (d) using the divergence theorem on the term containing the gradient of the incoming pressure, (7) reduces to the following form:

$$\int_{t_1}^{t_2}\left(-\rho_s d\int_\Gamma(\ddot v\delta v+\ddot w\delta w)d\lambda+\frac{\rho}{c^2}\int_{\Omega^f}\ddot\psi\delta\psi\,d\Omega-\frac{Ed}{1-\nu^2}\frac{1}{a^2}\int_\Gamma[(v_\phi+w)(\delta v_\phi+\delta w)+\beta^2(w_{\phi\phi}-v_\phi)(\delta w_{\phi\phi}-\delta v_\phi)]d\lambda\right.$$
$$+\rho\int_{\Omega^f}\nabla\psi\cdot\nabla\delta\psi\,d\Omega+\rho\int_\Gamma\dot\psi\delta w\,d\lambda+\rho\int_\Gamma\dot w\delta\psi\,d\lambda-\rho\int_{\Gamma^f}\mathcal{F}[\psi]\delta\psi\,d\lambda\Big)dt$$
$$=\int_{t_1}^{t_2}\left\{\int_\Gamma p^0\delta w\,d\lambda-\int_\Gamma\delta\psi\int_0^t p_n^0 dt\,d\lambda\right\}dt. \tag{9}$$

This variational form, which must hold for arbitrary δv, δw, and $\delta\psi$, will be the basis for the discretization process. To verify that (9) is the weak form of the structural acoustics problem under consideration we apply the divergence theorem in (9) on the terms that contain derivatives of the quantities δv, δw, and $\delta\psi$. After collecting like terms there results:

$$\int_{t_1}^{t_2}\left[\int_\Gamma\left(-\rho_s d\ddot v-\frac{Ed}{1-\nu^2}\frac{1}{a^2}[-v_{\phi\phi}-w_\phi+\beta^2(w_{\phi\phi\phi}-v_{\phi\phi})]\right)\delta v\,d\lambda+\int_\Gamma\left[-\rho_s d\ddot w-\frac{Ed}{1-\nu^2}\frac{1}{a^2}[v_\phi+w+\beta^2(w_{\phi\phi\phi\phi}-v_{\phi\phi\phi})]\right.\right.$$
$$\left.+\rho\dot\psi-p^0\right]\delta w\,d\lambda+\int_{\Omega^f}\left(-\rho\nabla^2\psi+\frac{\rho}{c^2}\ddot\psi\right)\delta\psi\,d\Omega+\int_\Gamma\left(-\rho\psi_n+\int_0^t p_n^0\,dt+\rho\dot w\right)\delta\psi\,d\lambda+\int_{\Gamma^f}[\psi_n-\mathcal{F}[\psi]]\delta\psi\,d\lambda\Big]dt$$
$$=0. \tag{10}$$

This expression will be satisfied for arbitrary δv, δw, and $\delta\psi$ if and only if:

$$\frac{a^2}{c_s^2}\ddot{v}-(1+\beta^2)v_{\phi\phi}-w_\phi+\beta^2 w_{\phi\phi\phi}=0, \text{ on } \Gamma, \tag{11a}$$

$$\frac{a^2}{c_s^2}\ddot{w}+v_\phi-\beta^2 v_{\phi\phi\phi}+w+\beta^2 w_{\phi\phi\phi\phi}+\frac{(1-\nu^2)a^2}{Ed}(p^0-\rho\dot{\psi}) =0, \text{ on } \Gamma, \tag{11b}$$

$$c^2\nabla^2\psi-\ddot{\psi}=0, \text{ in } \Omega^f, \tag{11c}$$

$$\dot{w}=\psi_n-\frac{1}{\rho}\int_0^t p_n^0\,dt, \text{ on } \Gamma, \tag{11d}$$

$$\psi_n-\mathcal{F}[\psi]=0, \text{ on } \Gamma^f, \tag{11e}$$

where $c_s=\sqrt{E/\rho_s(1-\nu^2)}$ is the compressional wave velocity in the shell.

Equations (11a) and (11b) are the equations of motion for the shell; (11c), the governing equation for the fluid, is the same as (3); and (11d), in view of (2a), ensures that the normal velocity of the shell is equal to that of the fluid across the interface Γ. Lastly, (11e) is the exact boundary condition on Γ^f. Notice that the last two conditions are natural, that is, they are satisfied automatically if the variational form (9) holds for arbitrary δv, δw, $\delta\psi$. Thus, we have established that the triad $[v,w,\psi]$ will be a solution of the exact structural acoustic problem defined by (11) if and only if (9) holds for arbitrary δv, δw, $\delta\psi$. Once ψ has been determined, the fluid velocity and pressure can be evaluated directly from (2).

In our approximate procedure, the exact absorbing boundary condition (11e) will be replaced by the approximate set of equations (6). [The implementation of the lower-order approximations (5a) or (5b) is straightforward.] To introduce (6) into the variational form (9) it suffices to replace the term that contains the exact value $\mathcal{F}$ of the normal derivative of ψ by its approximate counterpart and integrate the term containing second derivatives by parts. That is,

$$\begin{aligned}-\int_{\Gamma^f}\mathcal{F}[\psi]\delta\psi\,d\lambda &= \int_{\Gamma^f}\left(\frac{1}{c}\dot{\psi}-\frac{\kappa}{2}\psi-\frac{\kappa^2 c}{8\delta}\psi^{(1)}\right)\delta\psi\,d\lambda+\int_{\Gamma^f}\frac{c}{2\delta} \\ &\times\psi_\lambda^{(2)}\delta\psi_\lambda\,d\lambda+\int_{\Gamma^f}\frac{\kappa^2 c}{8\delta}\left(\psi-\psi^{(1)}-\frac{1}{\delta}\dot{\psi}^{(1)}\right) \\ &\times\delta\psi^{(1)}\,d\lambda+\int_{\Gamma^f}\frac{c}{2\delta}\left(\psi_\lambda-\psi_\lambda^{(2)}\right. \\ &\left.-\frac{1}{\delta}\dot{\psi}_\lambda^{(2)}\right)\delta\psi_\lambda^{(2)}\,d\lambda.\end{aligned} \tag{12}$$

It is important to observe that with the replacement (12) the variational operator in (9) will lead, upon spatial discretization, to a symmetric system of ordinary differential equations.

III. FINITE ELEMENT DISCRETIZATION

The spatial discretization of (9) with the replacement shown in (12) involves using standard finite element piecewise polynomial approximations for the displacements v and w on Γ, the velocity potential ψ in the closure $\bar{\Omega}^f$ of Ω^f, and the auxiliary function $\psi^{(1)}$ on Γ^f, as follows:

$$v(\mathbf{x},t)=\boldsymbol{\alpha}^T(\mathbf{x})\mathbf{v}(t), \tag{13a}$$

$$w(\mathbf{x},t)=\boldsymbol{\alpha}^T(\mathbf{x})\mathbf{w}(t), \tag{13b}$$

$$\psi(\mathbf{x},t)=\boldsymbol{\beta}^T(\mathbf{x})\boldsymbol{\psi}(t), \tag{13c}$$

$$\psi^{(1)}(\mathbf{x},t)=\boldsymbol{\gamma}^T(\mathbf{x})\boldsymbol{\psi}^{(1)}(t), \tag{13d}$$

in which, $\boldsymbol{\alpha}$, $\boldsymbol{\beta}$, and $\boldsymbol{\gamma}$ are vectors of global shape functions; $\mathbf{v}$, $\mathbf{w}$, $\boldsymbol{\psi}$, and $\boldsymbol{\psi}^{(1)}$ are the unknown nodal displacements, potential velocities, and auxiliary functions, defined over Γ, $\bar{\Omega}^f$, and Γ^f, initially at rest. The global shape functions $\boldsymbol{\alpha}(\mathbf{x})$ have continuous first derivatives on Γ; $\boldsymbol{\beta}(\mathbf{x})$ is continuous over $\bar{\Omega}^f$, and $\boldsymbol{\gamma}(\mathbf{x})$ corresponds to the restriction to Γ^f of $\boldsymbol{\beta}(\mathbf{x})$. On the other hand, since ψ and $\psi^{(2)}$ are related only through their second tangential derivatives, we express the tangential derivative of $\psi^{(2)}$ via:

$$\psi_\lambda^{(2)}(\mathbf{x},t)=\boldsymbol{\zeta}^T(\mathbf{x})\boldsymbol{\eta}(t), \tag{13e}$$

rather than approximating $\psi^{(2)}$ directly, in order to avoid singular matrices in later calculations. Here, $\zeta(\mathbf{x})$ need be only piecewise continuous over Γ^f.

The corresponding virtual quantities $\delta v(\mathbf{x})$, $\delta w(\mathbf{x})$, $\delta\psi(\mathbf{x})$, $\delta\psi^{(1)}(\mathbf{x})$, and $\delta\psi_\lambda^{(2)}(\mathbf{x})$ are approximated by the same global functions as their respective trial functions, i.e.,

$$\delta v(\mathbf{x})=\boldsymbol{\alpha}^T(\mathbf{x})\delta\mathbf{v}, \tag{14a}$$

$$\delta w(\mathbf{x})=\boldsymbol{\alpha}^T(\mathbf{x})\delta\mathbf{w}, \tag{14b}$$

$$\delta\psi(\mathbf{x})=\boldsymbol{\beta}^T(\mathbf{x})\delta\boldsymbol{\psi}, \tag{14c}$$

$$\delta\psi^{(1)}(\mathbf{x})=\boldsymbol{\gamma}^T(\mathbf{x})\delta\boldsymbol{\psi}^{(1)}, \tag{14d}$$

$$\delta\psi_\lambda^{(2)}(\mathbf{x})=\boldsymbol{\zeta}^T(\mathbf{x})\delta\boldsymbol{\eta}. \tag{14e}$$

After substituting (13) and (14) into (9) with (12), and noting that $\delta\mathbf{v}$, $\delta\mathbf{w}$, $\delta\boldsymbol{\psi}$, $\delta\boldsymbol{\psi}^{(1)}$, and $\delta\boldsymbol{\eta}$ are arbitrary, there results a system of ordinary differential equations with the following structure:

$$\boldsymbol{M}\ddot{\mathbf{U}}+\boldsymbol{C}\dot{\mathbf{U}}+\boldsymbol{K}\mathbf{U}=\mathbf{F}, \tag{15}$$

where, $\mathbf{U}^T=(\mathbf{v}^T,\mathbf{w}^T,\boldsymbol{\psi}_\Gamma^T,\boldsymbol{\psi}_{\Omega^f}^T,\boldsymbol{\psi}_{\Gamma^f}^T,\boldsymbol{\psi}^{(1)^T},\boldsymbol{\eta}^T)$, and $\boldsymbol{\psi}_\Gamma$, $\boldsymbol{\psi}_{\Omega^f}$, and $\boldsymbol{\psi}_{\Gamma^f}$ denote partitions of ψ over Γ, Ω^f, and Γ^f, respectively; M, C, and K are the mass, damping, and stiffness matrices of the system, and $\mathbf{F}(t)$ represents the effective wave excitation.

The matrices M, C, and K have the following form:

$$M=\begin{bmatrix} M^s_{vv} & 0 & 0 & 0 & 0 & 0 & 0 \\ 0 & M^s_{ww} & 0 & 0 & 0 & 0 & 0 \\ 0 & 0 & M^f_{\psi_\Gamma\psi_\Gamma} & M^f_{\psi_\Gamma\psi_{\Omega^f}} & 0 & 0 & 0 \\ 0 & 0 & M^f_{\psi_\Omega/\psi_\Gamma} & M^f_{\psi_\Omega/\psi_{\Omega^f}} & M^f_{\psi_\Omega/\psi_{\Gamma^f}} & 0 & 0 \\ 0 & 0 & 0 & M^f_{\psi_\Gamma/\psi_{\Omega^f}} & M^f_{\psi_\Gamma/\psi_{\Gamma^f}} & 0 & 0 \\ 0 & 0 & 0 & 0 & 0 & 0 & 0 \\ 0 & 0 & 0 & 0 & 0 & 0 & 0 \end{bmatrix}, \tag{16a}$$

$$C=\begin{bmatrix} 0 & 0 & 0 & 0 & 0 & 0 & 0 \\ 0 & 0 & C^{sf}_{w\psi_\Gamma} & 0 & 0 & 0 & 0 \\ 0 & C^{fs}_{\psi_\Gamma w} & 0 & 0 & 0 & 0 & 0 \\ 0 & 0 & 0 & 0 & 0 & 0 & 0 \\ 0 & 0 & 0 & 0 & C^a_{\psi_\Gamma/\psi_{\Gamma^f}} & 0 & 0 \\ 0 & 0 & 0 & 0 & 0 & C^a_{\psi^{(1)}\psi^{(1)}} & 0 \\ 0 & 0 & 0 & 0 & 0 & 0 & C^a_{\eta\eta} \end{bmatrix}, \tag{16b}$$

$$K=\begin{bmatrix} K^s_{vv} & K^s_{vw} & 0 & 0 & 0 & 0 & 0 \\ K^s_{wv} & K^s_{ww} & 0 & 0 & 0 & 0 & 0 \\ 0 & 0 & K^f_{\psi_\Gamma\psi_\Gamma} & K^f_{\psi_\Gamma\psi_{\Omega^f}} & 0 & 0 & 0 \\ 0 & 0 & K^f_{\psi_\Omega/\psi_\Gamma} & K^f_{\psi_\Omega/\psi_{\Omega^f}} & K^f_{\psi_\Omega/\psi_{\Gamma^f}} & 0 & 0 \\ 0 & 0 & 0 & K^f_{\psi_\Gamma/\psi_{\Omega^f}} & K^f_{\psi_\Gamma/\psi_{\Gamma^f}}+K^a_{\psi_\Gamma/\psi_{\Gamma^f}} & K^a_{\psi_\Gamma/\psi^{(1)}} & K^a_{\psi_\Gamma/\eta} \\ 0 & 0 & 0 & 0 & K^a_{\psi^{(1)}\psi_{\Gamma^f}} & K^a_{\psi^{(1)}\psi^{(1)}} & 0 \\ 0 & 0 & 0 & 0 & K^a_{\eta\psi_{\Gamma^f}} & 0 & K^a_{\eta\eta} \end{bmatrix}. \tag{16c}$$

The matrices M and K consist of three sets of block-diagonal matrices, each representing a different part of the system. The individual matrices within each block are designated by the superscripts s, f, or a, to indicate explicitly that they correspond to the structure (shell), the fluid, or the absorbing boundary. Thus the top left blocks are the standard mass and stiffness matrices associated with the shell, the middle blocks contain the corresponding sets for the fluid, and the bottom right block in (16b) and (16c) represents the effective damping and stiffness of the absorbing boundary.

Notice that the only coupling in the M and K matrices occurs between the fluid and the absorbing boundary. The shell and the fluid are coupled only through submatrices $C^{sf}_{w\psi_\Gamma}$ and $C^{fs}_{\psi_\Gamma w}$ of the matrix C. From (9), (13b), and (13c) these matrices are defined by

$$C^{sf}_{w\psi_\Gamma}=(C^{fs}_{\psi_\Gamma w})^T=\rho\int_\Gamma \alpha\beta^T\,d\lambda. \tag{17}$$

[Corresponding expressions for all the other submatrices that appear in (16) can be obtained readily from (9) with (12) and (13).]

Even though the submatrices $C^{sf}_{w\psi_\Gamma}$ and $C^{fs}_{\psi_\Gamma w}$ operate on the first derivative of U there is no energy dissipation associated with them since the idealized structure has been taken to be undamped and the fluid is inviscid. The only damping in the actual, unbounded, system comes from the radiated energy, which, in our formulation, is modeled through the bottom right block of C associated with the absorbing boundary.

From (15) and (16) it is seen that the absorbing boundary is characterized completely by the damping and stiffness matrices C^a and K^a, defined by

$$C^a=\begin{bmatrix} C^a_{\psi_\Gamma/\psi_{\Gamma^f}} & 0 & 0 \\ 0 & C^a_{\psi^{(1)}\psi^{(1)}} & 0 \\ 0 & 0 & C^a_{\eta\eta} \end{bmatrix},$$

$$K^a=\begin{bmatrix} K^a_{\psi_\Gamma/\psi_{\Gamma^f}} & K^a_{\psi_\Gamma/\psi^{(1)}} & K^a_{\psi_\Gamma/\eta} \\ K^a_{\psi^{(1)}\psi_{\Gamma^f}} & K^a_{\psi^{(1)}\psi^{(1)}} & 0 \\ K^a_{\eta\psi_{\Gamma^f}} & 0 & K^a_{\eta\eta} \end{bmatrix}, \tag{18}$$

as there is no inertia associated with our approximate absorbing boundary. Since C^a and K^a are local and symmetric they can be constructed element by element and incorporated into the equations of motion by standard assembly techniques using existing finite element software. All that is necessary is to incorporate the element matrices c^a and k^a corresponding to the global C^a and K^a into the finite element library of an existing software package for interior problems. The same finite element software package can then be used to solve the complete system of equations (15), in either assembled form, node-by-node, or element-by-element, by means of its own step-by-step time integrator.

To illustrate that the element matrices c^a and k^a have, indeed, a simple form, we provide below the corresponding explicit element matrices for the particular case of a circular absorbing boundary modeled by piecewise linear isoparametric elements:

$$k^a=\frac{1}{48}\begin{bmatrix} 8h & 4h & -2h & -h & -12R & -12R \\ 4h & 8h & -h & -2h & 12R & 12R \\ -2h & -h & 2h & h & 0 & 0 \\ -h & -2h & h & 2h & 0 & 0 \\ -12R & 12R & 0 & 0 & -8R^2h & -4R^2h \\ -12R & 12R & 0 & 0 & -4R^2h & -8R^2h \end{bmatrix}, \tag{19a}$$

$$c^a=\frac{Rh}{48c}\begin{bmatrix} 16 & 8 & 0 & 0 & 0 & 0 \\ 8 & 16 & 0 & 0 & 0 & 0 \\ 0 & 0 & 2 & 1 & 0 & 0 \\ 0 & 0 & 1 & 2 & 0 & 0 \\ 0 & 0 & 0 & 0 & -8R^2 & -4R^2 \\ 0 & 0 & 0 & 0 & -4R^2 & -8R^2 \end{bmatrix}, \tag{19b}$$

where h denotes the element length and R is the radius of the absorbing boundary (Fig. 2). These matrices correspond to the specific value of $\delta=c/R(=4\delta_{cr})$ in (12), thus ensuring the stability of the absorbing boundary condition, and hence, of the entire system (16).

The (6×6) matrices in (19) are associated with the six degrees of freedom corresponding to the nodal values of the three variables $\psi_{\Gamma f}$, $\psi^{(1)}$, and $\psi^{(2)}_{\lambda}$ at each end of a two-noded linear element. This impedance element can also be viewed as a six-noded element with one degree-of-freedom per node, as per Fig. 2. The potential function $\psi_{\Gamma f}$ is associated with the nodes 1 and 2, whereas the auxiliary variables $\psi^{(1)}$ and $\psi^{(2)}_{\lambda}$ are associated with the nodes 3, 4 and 5, 6, respectively. It should be observed that even though the six nodes in the impedance element are shown in Fig. 2 as occupying distinct locations for ease of visualization, in reality nodes 3, 5 and 4, 6 coincide with nodes 1 and 2, respectively. Alternative matrices k^a and c^a corresponding to higher-order polynomial approximations can be constructed readily by selecting different shape functions in (13).

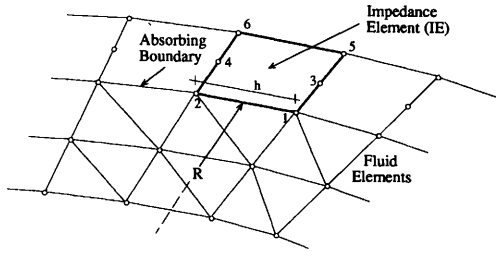

FIG. 2. Impedance element.

It should also be noted that except for a change in the physical meaning of the nodal quantities, the structure of the absorbing boundary element is such that it can be used with either potential-based formulations, as the one presented herein, or with pressure-based formulations where the total pressure is the primary unknown field quantity within the fluid domain. In the latter case, however, the symmetry of the formulation is lost. We complete our description of the finite element discretization by giving some details about the forcing function $\mathbf{F}$ in (15). From (9) it is clear that $\mathbf{F}$ has nonzero values only for the degrees of freedom associated with the nodal shell radial displacements and the fluid velocity potential, i.e., $\mathbf{F}^T=(0^T,\mathbf{F}^T_w,\mathbf{F}^T_{\psi_\Gamma},0^T,0^T,0^T,0^T)$, where

$$\mathbf{F}_w(t)=\int_\Gamma p^0\boldsymbol{\alpha}\,ds, \tag{20a}$$

$$\mathbf{F}_{\psi_\Gamma}(t)=\int_\Gamma\int_0^t p^0_n\,dt\,\boldsymbol{\beta}\,ds. \tag{20b}$$

We recall that for the scattering problem discussed thus far p^0 and p^0_n are the pressure and the normal derivative of the

pressure of the prescribed incident wave on the wet surface Γ. If one is interested in the radiation problem, one need only interpret p^0 in (20a) as the normal pressure applied directly on the shell and set $\mathbf{F}_{\psi_\Gamma}$ equal to zero. The radiated pressure p^r in the fluid can be obtained directly from the solution of (15) as

$$p^r = -\rho\dot{\psi}. \tag{21}$$

Clearly, (15) can be solved by standard step-by-step integration schemes; in this paper the numerical results are obtained by the trapezoidal rule. In the case of a time-harmonic steady-state excitation $\mathbf{F}=\bar{\mathbf{F}}e^{i\omega t}$, (15) can be used directly in the frequency domain by solving the system of algebraic equations

$$(-\omega^2 M + i\omega C + K)\bar{\mathbf{U}} = \bar{\mathbf{F}}, \tag{22}$$

which results from seeking a solution of the form $\mathbf{U}=\bar{\mathbf{U}}e^{i\omega t}$.

IV. NUMERICAL EXAMPLES

Our numerical experiments aim primarily at assessing the accuracy and validity of the suggested methodology with particular focus in the performance of the impedance element (IE) in the transient regime. To this end simple canonical systems are considered in two specific situations. One corresponds to a homogeneous elastic shell submerged in water and the other consists of the same homogeneous shell but with an added concentrated line mass equal to one half the mass of the shell, per unit length. The relative properties for the homogeneous shell are: $c_s/c=3.53$, $\rho_s/\rho=7.65$, $\nu=0.3$, and $d/a=0.01$.

We consider both an exterior excitation in the form of a traveling plane wave that impinges upon the shell (scattering problem) and an interior excitation in the form of a line force acting on the shell (radiation problem). For completeness, we also consider the scattering problem for the limiting rigid case ($c_s/c=\infty$). In all cases the time signal is represented by a finite-duration modified Ricker[20] pulse as shown in Fig. 3(a), where ω_r is the dominant frequency of the excitation; a unit peak amplitude has been considered in this figure. The amplitude of the corresponding Fourier transform is shown in Fig. 3(b). The numerical results in this section were obtained by using piecewise cubic Hermite polynomials for the shell, eight-noded quadratic elements for the fluid, and nine-noded quadratic elements for the boundary elements.

Figure 4 depicts the normalized backscattered pressure directly on a rigid circular scatterer as a function of normalized time, for different values of the dimensionless wave number $k_r a$, where $k_r=\omega_r/c$ is the dominant wave number of the Ricker pulse. Notice the different horizontal and vertical scales for the various wave numbers. The dotted lines represent the numerical solutions of the problem when the second-order circular absorbing boundary (6) is placed at a distance $r/a=1.2$ from the center of the scatterer, i.e., at only $0.2a$ from the wet surface of the scatterer. (The number of radial and angular elements, n_r and n_θ, used for each wave number are indicated in the figure caption.) These solutions are to be compared against the corresponding exact solutions, shown by solid lines, obtained by inversion via FFT of the exact frequency-domain solution of the original exterior problem. The two sets of curves essentially agree with each other; by moving farther the absorbing boundary to $r/a=1.6$ the two solutions become indistinguishable. Also shown for comparison in this figure are the solutions obtained by using the plane wave (PWA) and spring-dashpot (SD) approximations for the absorbing boundary, (5a) and (5b), respectively. Clearly, the PWA and SD approximations are unacceptable at low frequencies. Their accuracy increases with the wave number $k_r a$, but in all cases the solution for the impedance element (IE) is closer to the exact solution, at negligible additional computational cost.

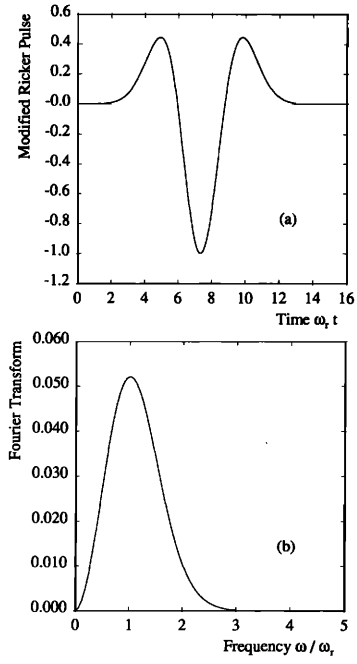

FIG. 3. (a) Finite-duration modified Ricker pulse; (b) Fourier transform of (a).

Next we consider the response of the homogeneous shell as well as that of the shell with the concentrated line mass to an incident plane wave for a dominant wave number $k_r a=4$. Here and in the remainder of the paper we use only the second-order boundary condition (6). The top half of Fig. 5 shows the normalized scattered pressure computed at different points on the wet surface of the shell and within the fluid on the absorbing boundary. (The points are identified by solid bullets in the inserts shown in the figure.) The boundary is located at $r/a=1.2$ and the incident wave propagates from east to west as shown. The phase lag between the response at the various points is clear from this figure. In addition to the numerical approximations the response at the same points has also been computed by inverting the exact frequency-domain solution via the FFT. (The calculations were carried out for values of tc/a up to 100 with a time step $\Delta tc/a=0.1$, but here the response is shown only up to 16 since the response practically dies out beyond this value, especially for the homogeneous shell.) Again, the two approximate and the

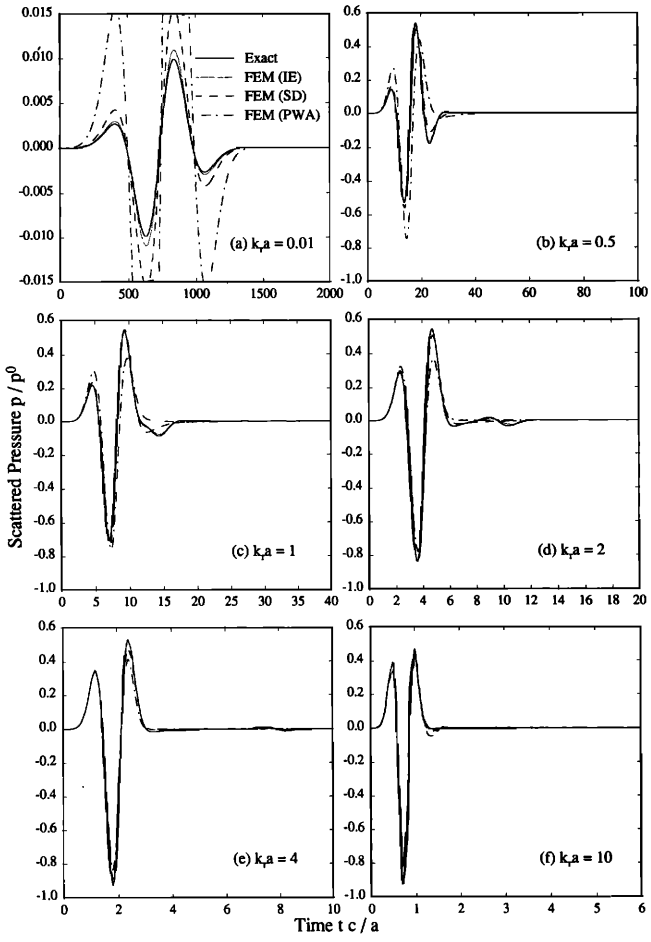

FIG. 4. Backscattered pressure directly on a rigid scatterer, exact and FEM solutions; (a) $n_r=2$, $n_\theta=12$, (b) $n_r=2$, $n_\theta=12$, (c) $n_r=2$, $n_\theta=16$, (d) $n_r=2$, $n_\theta=32$, (e) $n_r=2$, $n_\theta=32$, (f) $n_r=4$, $n_\theta=64$.

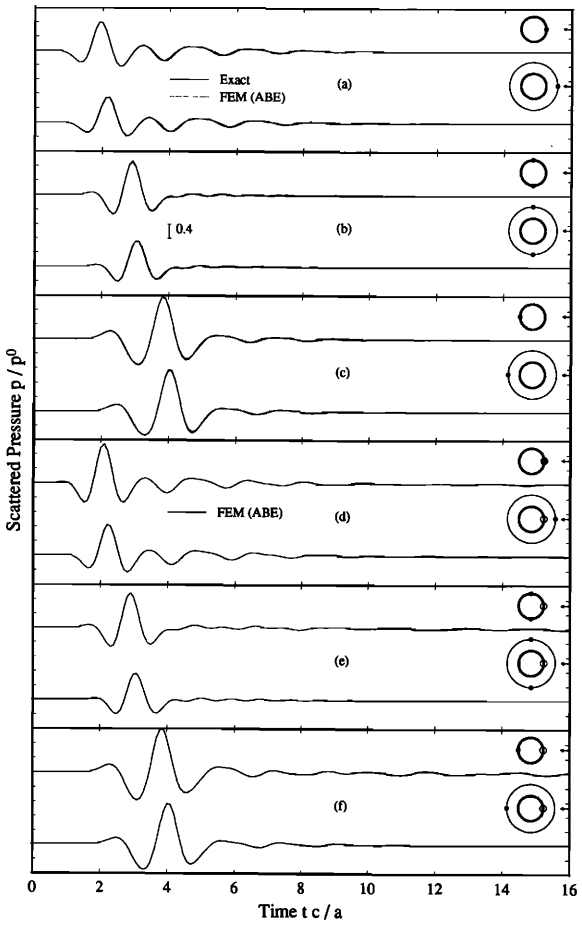

FIG. 5. Scattered pressure at various points (denoted by solid bullets) on and near a shell due to an incident plane wave; $n_r=8$, $n_\theta=16$, $r/a=1.2$, $k_sa=4$; (a), (b), (c) homogeneous shell; (d), (e), (f) shell with concentrated line mass (inhomogeneous shell).

exact solutions practically coincide. The corresponding approximate solutions for the shell with the concentrated mass (denoted by an open circle) are shown on the bottom half of Fig. 5. No significant differences are apparent in the scattered pressure either on the wet surface or within the fluid itself, due to the added mass. Interestingly, one can recover the normalized frequency spectrum that characterizes a particular structure by applying an FFT to the transient response and then dividing the result for each frequency by the corresponding amplitude of the Fourier transform of the Ricker pulse [Fig. 3(b)]. The result of this transformation on the scattered pressure is shown on Figs. 6 and 7 for the uniform shell and the shell with the concentrated mass, respectively. It is noteworthy that the scattered pressure at a distance of only $0.2a$ from the scatterer has the same characteristics as the far-field response, including the scallop-like shape of the backscattered pressure with dips at normalized frequencies $ka=nc_s/c$ ($n=1,2,...$). Here $k=\omega/c$, and the dips represent a dynamic absorber effect corresponding to the natural frequencies of the shell *in vacuo* when it is constrained to deform only tangentially (without deforming in the radial direction), i.e., essentially as a confined membrane. Several small peaks may be observed directly on the surface of the shell, corresponding to resonant frequencies of the shell–fluid system. The presence of resonant frequencies is more pronounced for the shell with a mass (Fig. 7). Here resonant frequencies are quite distinct, though the peaks are highly attenuated, away from the shell.

Figures 8 and 9 pertain to the radiated pressure field generated within the fluid when a horizontal concentrated line load acts directly on the shell, as indicated in the inserts. Results for the homogeneous shell are shown on Fig. 8 while those on Fig. 9 are for the shell with a concentrated mass. These results were obtained by placing the absorbing boundary at $r/a=1.6$. The need for using a larger buffer zone relative to that used for the scattering problems ($r/a=1.2$) is that higher "modes" are excited by the applied load than by an incident wave, within the frequency range of interest. To verify that $r/a=1.6$ provides a sufficient buffer the same problems were solved a second time, but with the absorbing boundary at $r/a=2$, with no change in the results. The most striking difference between the radiation and the scattering problems is, of course, the long duration and large amplitude of the radiated pressure directly outside the shell. Another interesting feature is that the added inertia due to the concentrated mass has a significant effect in reducing the amplitude of the radiated pressure on the wet surface. By contrast with the homoge-

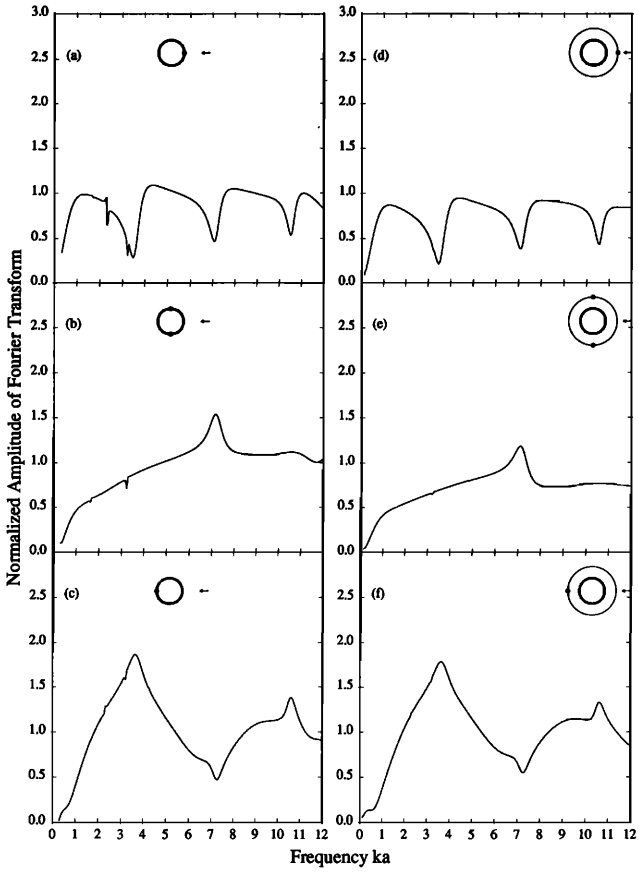

FIG. 6. Normalized Fourier transform of the scattered pressure for the homogeneous shell [Fig. 5(a), (b), (c)]; (a), (b), (c) points on surface; (d), (e), (f) points at $r/a=1.2$.

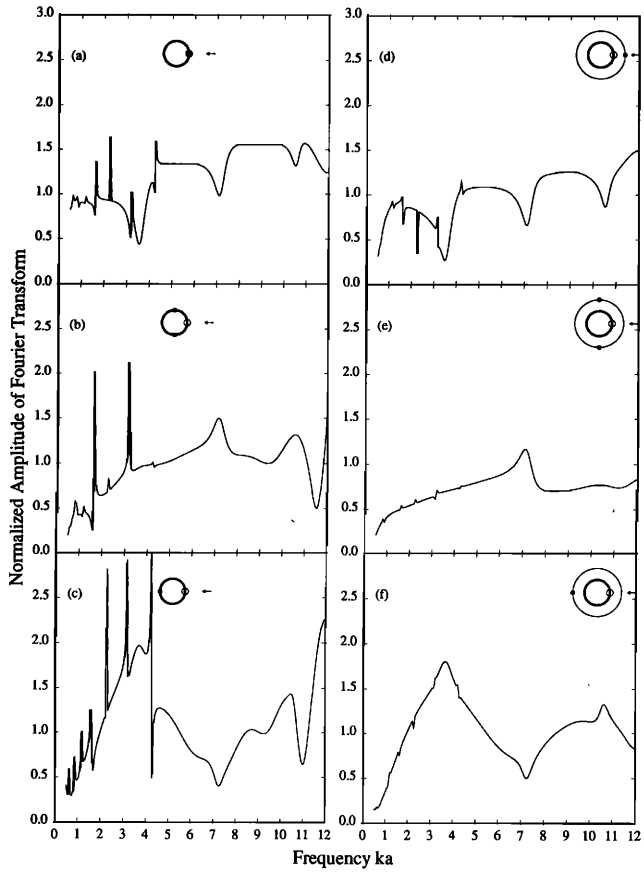

FIG. 7. Normalized Fourier transform of the scattered pressure for the inhomogeneous shell [Fig. 5(c), (d), (e)]; (a), (b), (c) points on surface; (d), (e), (f) points at $r/a=1.2$.

neous shell, the interference provided by the concentrated mass causes the waves circumnavigating the shell to be radiated more strongly into the fluid.

Figure 10 shows the radial and tangential displacements at various points of the homogeneous shell corresponding to the radiation problem for the homogeneous shell. Observe that the shape of the initial pulse of radial displacement at the point of application of the load is essentially equal to that obtained by integrating with respect to time the expression for the applied pressure, as expected, and that after a period of relative quiet there is a constructive interference of the waves propagating around the circumference. The tangential displacement is shown only at the north and south points as the east and west points are nodal points. Notice also the difference in scale between the radial and tangential displacements, confirming that the response of the shell is predominantly in the radial direction.

We next perform the same normalized FFT procedure on the results shown in Figs. 9 and 10 for the radiation problems as we did previously for the scattering problem. This process results in Figs. 11 and 12, respectively. Contrary to the results in Fig. 7 here it is seen that the radiated pressure on the wet surface exhibits a discrete set of large peaks. These correspond precisely to the resonant frequencies of the shell–fluid system, i.e., the frequencies for which the real part of the system's impedance vanishes. Warburton[24] has given the following formula for approximating the various resonant frequencies, ω_n of the immersed shell, under the assumption that the modes of the shell immersed in the acoustic fluid are the same as those for the shell *in vacuo*:

$$\omega_n=\Omega_n\left(1+\frac{n}{n^2+1}\frac{\rho}{\rho_s}\frac{a}{d}\right)^{-1/2}. \tag{23}$$

Here Ω_n is the nth natural frequency of the shell *in vacuo*. For ka between 0.8 and 4 the locations of the peaks of the radiated pressure generated by the homogeneous shell practically coincide with the values given by the preceding formula, thus providing another verification of the validity of the new methodology. However, the accuracy gradually degrades as the wave number, and hence the mode number, increases, due to the limited number of elements used in the angular direction. For the shell with the concentrated mass the resonant frequencies are, as expected, slightly lower than the corresponding ones for the homogeneous shell. Observe that the resonant frequencies corresponding to the odd number of wavelengths are absent from the records for the north and south points, as these are nodal points. However, once the concentrated mass is introduced these are no longer nodal points.

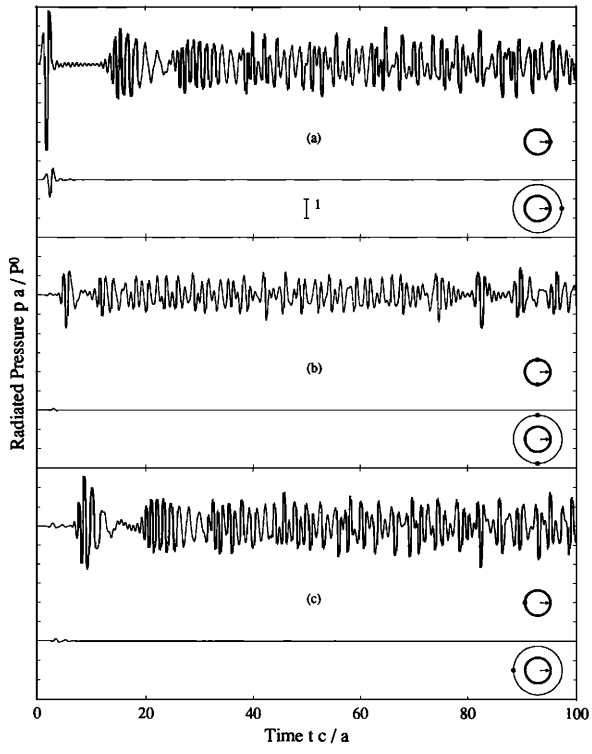

FIG. 8. Radiated pressure at various points (denoted by solid bullets) of a homogeneous shell due to a line load applied directly on the shell; $n_r=8$, $n_\theta=64$, $r/a=1.6$, $k_f a=4$.

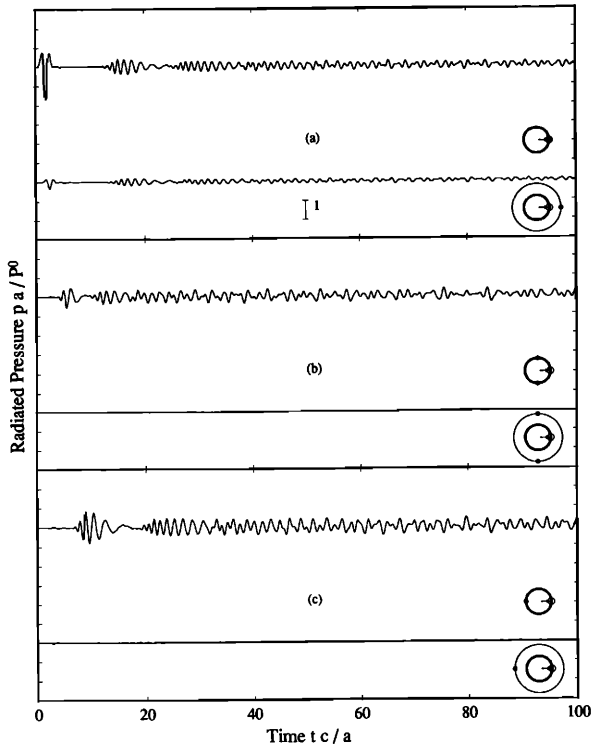

FIG. 9. Radiated pressure at various points (denoted by solid bullets) of the inhomogeneous shell due to a line load applied directly on the shell; $n_r=8$, $n_\theta=64$, $r/a=1.6$, $k_f a=4$.

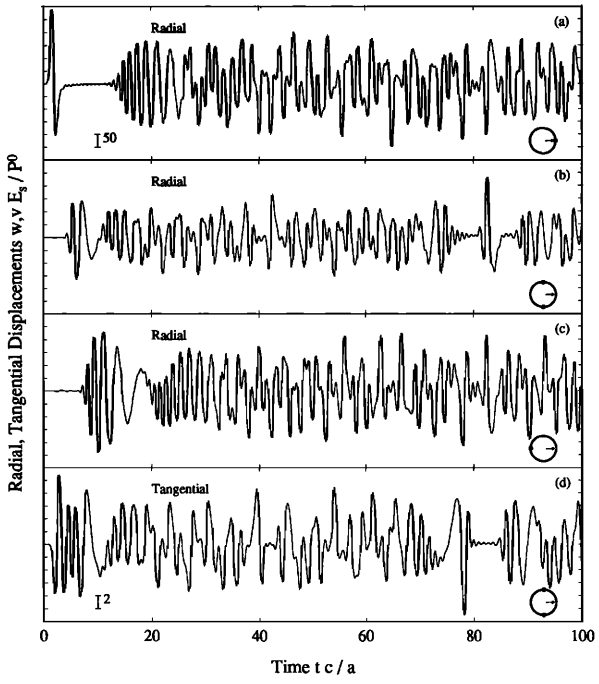

FIG. 10. Normalized radial and tangential displacements at various points (denoted by solid bullets) of a homogeneous shell loaded with a line load; $n_r=8$, $n_\theta=64$, $r/a=1.6$, $k_f a=4$; (a), (b), (c) radial displacements; (d) tangential displacement.

Turning to the radiated pressure within the fluid one can make the following observations from Figs. 11(d), (e), (f), and 12(d), (e), (f),

(1) Even at a short distance of $0.6a$ from the perfect shell, the resonant behavior of the shell is no longer discernible [Fig. 11(d), (e), and (f)]. While this is the expected behavior in the far field, it is somewhat interesting that it is already apparent near the shell.

(2) For the scattering problem, we mentioned earlier that within the frequency range considered, the resonant frequencies of the fluid–structure system play no significant role in the response. Only the constrained tangential frequencies of the shell *in vacuo* are relevant. It is interesting that the same is true for the radiation problem for the homogeneous shell for a listener located even at a short distance away from the shell.

(3) The behavior is drastically different for the shell with a concentrated mass. In this case the radiated wave carries clear information about all the resonant frequencies of the shell–fluid system.

(4) By comparing Fig. 12 with Fig. 7 one is led to conclude that for purposes of structural identification the radiated pressure may be more useful than the scattered pressure. The resonant frequencies of the fluid–structure system, which may be regarded as the system's signature, can be determined quite accurately from the records of the radiated pressure obtained at a single listening point. The noise present in Figs. 6, 7, 11, and 12 at the lower end of the spectrum is mainly due to the truncation of the time signal for the inversion process.

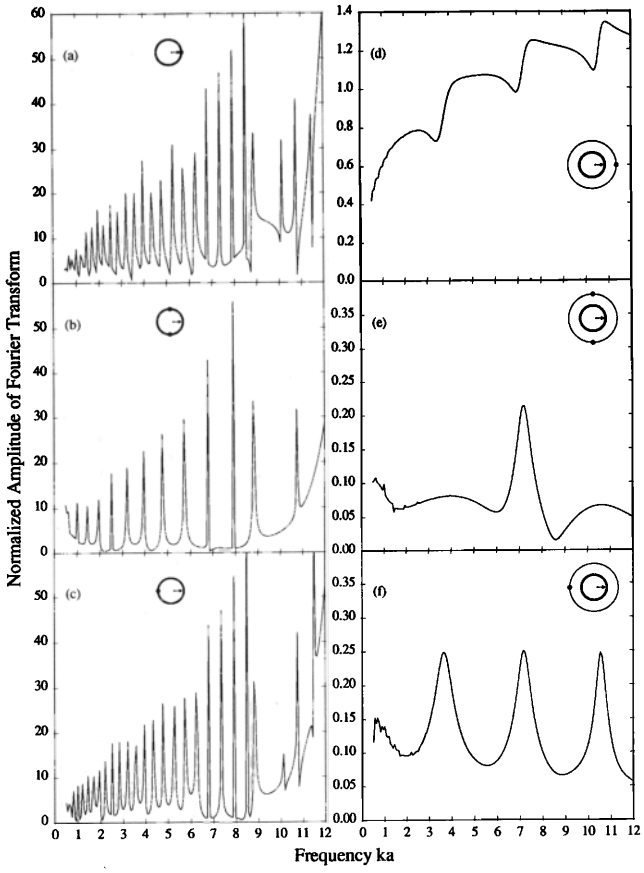

FIG. 11. Normalized Fourier transform of the radiated pressure for the homogeneous shell (Fig. 8); (a), (b), (c) points on surface; (d), (e), (f) points at $r/a=1.6$.

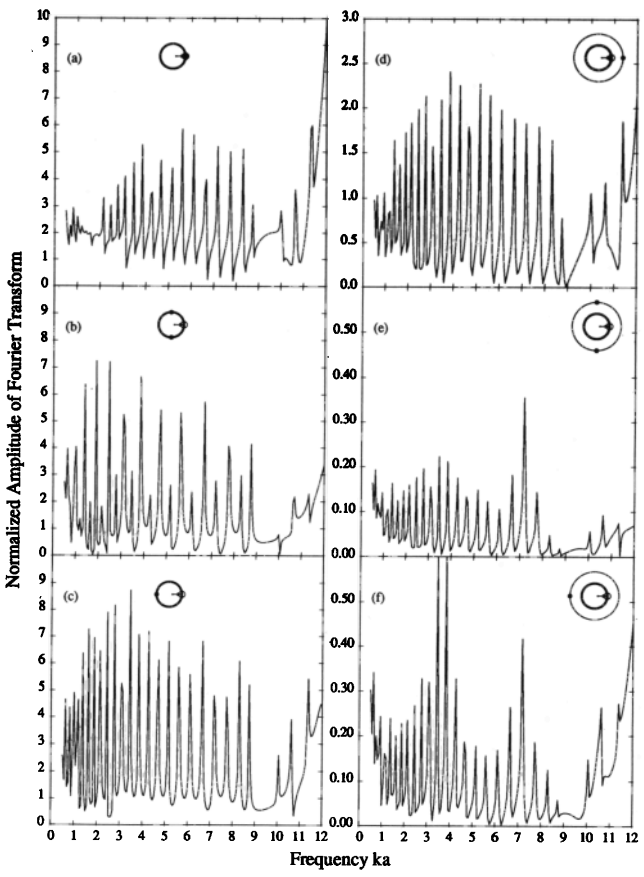

FIG. 12. Normalized Fourier transform of the radiated pressure for the inhomogeneous shell (Fig. 9); (a), (b), (c) points on surface; (d), (e), (f) points at $r/a=1.6$.

V. CONCLUDING REMARKS

In light of the excellent agreement between the approximate and exact solutions obtained for the test problems, it appears that the new methodology based on finite element spatial discretization, standard step-by-step time integration, and a novel absorbing boundary element, provides a practical and accurate means for solving complex transient radiation and scattering problems in structural acoustics directly in the time domain. This method can also be used for obtaining frequency domain solutions either directly by solving (22) for each frequency, or indirectly via FFTs as it was done herein. The novel absorbing boundary element permits one to retain the familiar form of the discretized equations of motion for the structure with their sparsity and symmetry intact. Since the element is completely represented by a pair of local symmetric stiffness and damping matrices, the entire procedure lends itself to easy incorporation into existing finite element codes for interior problems. It also allows for ready parallelization that will best exploit the main features of particular advanced architecture computers.

In this paper we have concentrated on the near-field behavior of the radiated and scattered pressure. Once this behavior has been established, one need consider only the fluid in order to determine the far-field behavior, using time-domain[7] or frequency-domain approaches. One of the major objectives of this paper was to describe the overall merits of the proposed methodology. For this reason canonical structures with simple geometries were used both in the theory and in the numerical illustrations. If, however, one uses the general theory of elastodynamics to model the submerged structure, the methodology can be applied directly to arbitrary elastic structures (damping characteristics can be introduced without difficulty). Also, the present study was restricted to the analysis of elastic structures submerged in a full space. The present formulation for the fluid, however, can be applied without modification to analyze a possible inelastic structure submerged in a half-space (free-surface or rigid bottom) provided the problem conditions are such that the fluid can still be idealized as a linear acoustic medium and the free-surface boundary condition can be approximated by a pressure release condition. Based on similar procedures, extensions to three-dimensional problems are also possible. These will be addressed in future communications. We hope this paper has helped show that the proposed methodology provides a computationally powerful tool that will assist in gaining physical insight and in solving large problems involving complex submerged structures.

ACKNOWLEDGMENTS

The work of L. F. Kallivokas was supported by a fellowship from Swanson Analysis Systems, Inc. We are grateful for this support.

[1] R. A. Jeans and I. C. Mathews, "Solution of fluid-structure interaction problems using a coupled finite element and variational boundary element technique," J. Acoust. Soc. Am. **88**, 2459–2466 (1990).

[2] X. Zeng, L. F. Kallivokas, and J. Bielak, "Stable localized symmetric integral equation method for acoustic scattering problems," J. Acoust. Soc. Am. **91**, 2510–2518 (1992).

[3] X. Zeng, J. Bielak, and R. C. MacCamy, "Unified symmetric finite element and boundary integral variational coupling methods for linear fluid-structure interaction," Num. Meth. Part. Diff. Equation **8**, 451–467 (1992).

[4] J. Bjarnason, J. D. Achenbach, and T. Igusa, "Acoustic radiation from a cylindrical shell with an internal plate," Wave Motion **15**, 23–41 (1992).

[5] D. Givoli, "Non-reflecting boundary conditions: a review," J. Comput. Phys. **94**(1), 1–29 (1991).

[6] B. Engquist and A. Majda, "Radiation boundary conditions for acoustic and elastic wave calculations," Comm. Pure Appl. Math. **32**(3), 313–357 (1979).

[7] A. Bayliss and E. Turkel, "Radiation boundary conditions for wave-like equations," Comm. Pure Appl. Math. **33**(6), 707–725 (1980).

[8] P. M. Pinsky, L. L. Thompson, and N. N. Abboud, "Local high-order radiation boundary conditions for the two-dimensional time-dependent structural acoustics problem," J. Acoust. Soc. Am. **91**, 1320–1335 (1992).

[9] P. M. Pinsky and N. N. Abboud, "Transient finite element analysis of the exterior structural acoustics problem," J. Vib. Acoust. **112**, 245–256 (1990).

[10] P. M. Pinsky and N. N. Abboud, "Finite element solution of the transient exterior structural acoustics problem based on the use of radially asymptotic boundary operators," Comput. Methods Appl. Mech. Eng. **85**, 311–348 (1991).

[11] G. C. Everstine, "A symmetric potential formulation for fluid-structure interaction," ASME J. Sound and Vib. **79**(1), 157–160 (1981).

[12] S. D. O'Regan and F. DiMaggio, "Dynamic response of submerged shells with appendages," J. Eng. Mech. **116**(10), 2275–2292 (1990).

[13] T. L. Geers, "Residual potential and approximate methods for three-dimensional fluid-structure interaction problems," J. Acoust. Soc. Am. **49**, 1505–1510 (1971).

[14] T. L. Geers, "Doubly asymptotic approximation for transient motions of submerged structures," J. Acoust. Soc. Am. **64**, 1500–1508 (1978).

[15] C. A. Felippa, "Top-down derivation of doubly asymptotic approximations for structure-fluid interaction analysis," in *Innovative Numerical Analysis for the Engineering Sciences*, edited by R. P. Shaw, J. Periaux, A. Chaudouet, J. Wu, C. Marino, and C. A. Brebbia (U.P. of Virginia, Charlottesville, 1980), pp. 79–88.

[16] T. L. Geers and C. A. Felippa, "Doubly asymptotic approximations for vibration analysis of submerged structures," J. Acoust. Soc. Am., **73**(4), 1152–1159 (1983).

[17] B. Nicolas-Vullierme, "A contribution to doubly asymptotic approximations: an operator top-down approach," *Numerical Techniques in Acoustic Radiation* (ASME, New York, 1989), NCA-Vol. 6, pp. 7–13.

[18] A. Barry, J. Bielak, and R. C. MacCamy, "On absorbing boundary conditions for wave propagation," J. Comput. Phys. **79**, 449–468 (1988).

[19] L. F. Kallivokas, J. Bielak, and R. C. MacCamy, "Symmetric local absorbing boundaries in time and space," J. Eng. Mech. **117**(9), 2027–2048 (1991).

[20] N. H. Ricker, *Transient Waves in Visco-elastic Media* (Elsevier, Amsterdam, The Netherlands, 1977).

[21] R. D. Mindlin and H. H. Bleich, "Response of an elastic cylindrical shell to a transverse, step shock wave," J. Appl. Mech. **20**, 189–195 (1953).

[22] G. A. Kriegsmann, A. Taflove, and K. R. Umashankar, "A new formulation of electromagnetic wave scattering using an on-surface radiation boundary condition approach," IEEE Trans. Antennas Propag. **AP-35**(2), 153–160 (1987).

[23] M. C. Junger and D. Feit, *Sound Structures, and Their Interaction* (MIT, Cambridge, MA, 1972).

[24] G. B. Warburton, "Vibration of a cylindrical shell in an acoustic medium," J. Mech. Eng. Sci. **3**, 69–79 (1961).